A DFT study of the catalytic ODH of *n*-hexane over a cluster model of vanadium oxide

Nkululeko E. Damoyi[a,*], Holger B. Friedrich[b], Gert H. Kruger[c], David J. Willock[d]

[a] Department of Chemistry, Mangosuthu University of Technology, Box 12363, Jacobs 4026, South Africa
[b] School of Chemistry and Physics, University of KwaZulu-Natal, Westville Campus, Private Bag X 54001, Durban 4000, South Africa
[c] Catalysis and Peptide Research Unit, School of Pharmacy, University of KwaZulu-Natal, Westville Campus, Private Bag X 54001, Durban 4000, South Africa
[d] School of Chemistry, Cardiff University, Park Place, Cardiff, NSW CF10 3AT, United Kingdom

ARTICLE INFO

Keywords:
DFT
ODH
RDS
Mechanism

ABSTRACT

Supported vanadium oxides are one of the most widely reported catalysts for the selective oxidative dehydrogenation (ODH) of alkanes to alkenes. These vanadium oxide catalysts contain at least three distinct O species classified by their coordination to the vanadium cations. The involvement in ODH of the different oxygen species is thought to follow the coordination environment with singly coordinated vanadyl V(V)=*O* being the most reactive. A quantitative understanding of the relative activity of the different oxygen species in vanadium oxides could inform catalyst design to further enhance productivity and selectivity in the ODH reaction. Here we use computational models based on hybrid density functional theory to study the mechanistic pathway for *n*-hexane to 1- and 2-hexene. We compare the potential energy surfaces calculated for these reactions initiated by β-H abstraction with H transfer to the vanadyl oxygen, V(V)=*O*, with that involving H transfer to a two-coordinate bridging O atom. An isolated $H_4V_2O_7$ cluster is used to represent the supported vanadium oxide catalyst so that the reactivity of oxygen species can be understood in the absence of support effects. Gibbs energy calculations were carried out at temperatures of 573, 673 and 773 K to mirror laboratory experimental conditions. We find that the rate-determining step (RDS) in the conversion of *n*-hexane to either alkene is associated with *n*-hexane interaction with $H_4V_2O_7$ through a secondary C─H bond. This leads to β-H abstraction with the calculated reaction barrier for abstraction by a V(V)=*O* ($\Delta E^{\ddagger}$ = +32.7 kcal mol^{-1}) significantly lower than that for the two-coordinate bridging O ($\Delta E^{\ddagger}$ = +43.9 kcal mol^{-1}). H-abstraction leads to reduction of one of the vanadium cations. Removal of the second H atom to form an alkene can follow several pathways. We have considered the second step leading to 2-hexene (γ-H abstraction) using either an adjacent V(V)=*O* on the reduced V(IV)-O-V(V) unit, a different active V(V)=*O* site on a fully oxidised cluster, or gas-phase molecular O_2. Our results show that the ODH process is likely to proceed via a Mars-van Krevelen redox mechanism. In a practical catalyst the results imply that catalyst activity will depend on the surface coverage of V(V)=*O* active sites and the *n*-hexane to gas-phase molecular oxygen ratio. In addition to the pathways leading to alkene products we have noted the formation of C─O bonds by the radical intermediate formed from the initial β-H abstraction. From this observation, we suggest that the low yields of 1- and 2-hexene (< 20%) obtained in our laboratory experiments with V_2O_5/MgO catalysts may be a result of the chemisorption properties of the radical intermediate ($\bullet C_6H_{13}$) on bridging or terminal O sites in the V(V)-O-V(V) units, leading to undesired products including oxygenates.

1. Introduction

Olefins are fundamental raw materials for many industrial processes such as the production of polypropylene, acrylonitrile, and propylene oxide [1]. Since non-oxidative dehydrogenation of alkanes is an endothermic and therefore energy intensive process, it suffers from low alkene yields due to catalyst coking; whereas the alternative, oxidative dehydrogenation (ODH), is exothermic because of the formation of water and does not lead to the formation of coke [2]. Presently, the main drawback in industrial processes for ODH of short alkanes is low selectivity to the desired alkenes because the products are prone to total oxidation by the catalysts [3]. Therefore, much current research in ODH

* Corresponding author.
E-mail address: damoyi@mut.ac.za (N.E. Damoyi).

of alkanes focuses on finding good catalysts with high selectivity to alkenes in competition with products in which oxygen has been inserted into the molecular structure.

Supported vanadium oxides are one of the best catalysts for the alkene selective ODH of propane [4–7]. Earlier experimental studies indicate that the selective oxidation of propane on vanadium oxides proceeds via a Mars-van Krevelen redox mechanism that involves the reduction of the metal oxide surface by the alkane with the formation of the alkene and water, followed by reoxidation of the surface through gas-phase oxygen [8]. Other studies [9–11] have described the reoxidation as involving the adsorption of gas-phase molecular oxygen on a vacancy, where one of the two O atoms eliminates the vacancy and other O atom migrates to the surface and re-oxidize a second vacancy. However, it is well known that, depending on the method of preparation, the vanadium surface may contain three types of lattice oxygen species, namely, (i) the singly coordinated V(V)=*O*, (ii) the two-coordinated bridging O, and (iii) the three-coordinated bridging O [12]. Experimentally, it is not clear how the reactivity of surface O for ODH reactions depends on its coordination to V in the surface. In addition, location and coordination of the reactive metal site is also very important, particularly for understanding the mechanism of such active metal sites with reactants and intermediates in ODH reactions on a molecular level [13]. Many researchers [14–16] have suggested the involvement of vanadyl V(V)=*O* oxygen as critical in hydrocarbon oxidation reactions, while others have mentioned the bridging O sites [17,18]. C– H bond activation on the three-coordinated bridging O site is the least likely, as this highly coordinated oxygen species is the most inert, [19] Hui et al. [12], have compared the reducibility of the three differently coordinated O atoms, and found that the singly coordinated V(V)=*O* is the most easily reduced of the three oxygen species on the surface and possesses the strongest electrophilic tendency, while the three-coordinated bridging O is the least reactive. RDS for C– H activation of propane has been proposed as the hydrogen abstraction by V(V)=*O* to form an isopropyl radical as an intermediate in the gas phase [20,21] which seems in good agreement with the preceding discussion of the reactivity of surface O species. In our previous studies of gas-phase activation of *n*-hexane by isolated H_3VO_4 species, we also found that RDS proceeds by *β*-hydrogen abstraction by V(V)=*O* to form the hexyl radical and a reduced V(IV) species [22]. In that study the size of the simulated vanadium complex meant that only the V(V)=*O* oxygen environment could be considered as the remaining O atoms coordinating to V were terminated by H atoms to give the correct valency to represent a surface V ion. This fits well with our experiments where we utilize the MgO support which is less involved in the catalytic mechanism as opposed to for example, Al_2O_3 and SiO_2 supports which are more involved [20]. In this contribution we extend our studies of using cluster models to investigate the vanadium oxide catalysed alkane ODH reaction to include both vanadyl V(V)=*O* and two coordinate O species. This allows the comparison of the reactivity of the V(V)=*O* and the two-coordinated bridging O and the differences quantified based on the computed reaction potential energy surface.

The aim of this study was to investigate and compare C–H bond activation of *n*-hexane by vanadyl and bridging O atoms in isolated $H_4V_2O_7$ species and characterise the possible intermediates that may lead to 1- and 2-hexene, by means of DFT calculations. The pathways that are likely to lead to other unsaturated alkenes, aromatics and carbon oxides are not part of this study. The calculations of relative energy changes, namely, the sum of electronic and zero-point energy change of activation ($\Delta E^{\ddagger}$), the sum of electronic and zero-point energy change (ΔE), the sum of electronic and thermal Gibbs energy change of activation ($\Delta G^{\ddagger}$), and the sum of electronic and thermal Gibbs energy change (ΔG), were performed for determination of the likely mechanistic pathway for the reaction.

2. Theoretical methodology

2.1. Computational details

DFT calculations were carried out using the GAUSSIAN 09 W program [23] installed on a cluster based at the Centre for High Performance Computing (CHPC) in Cape Town, South Africa. The UB3LYP hybrid correlation functional [24,25], and 6–311+*G*(d,p) basis set were employed for C, O and H atoms and the V atom was described using the relativistic Stuttgart ECPs and associated valence functions (ECP10MDF) [26,27]. Relaxed potential energy surface (PES) scans were utilised to get good initial structures for the transition state (TS) determinations and the TS structures were fully optimized without constraints. Intrinsic reaction coordinate (IRC) calculations, from the algorithm developed by Gonzàlez and Schlegel [28,29] were performed to confirm that each transition state connects two appropriate local minima on the reaction pathway. Calculation of frequencies for all structures was also used to confirm transition states and to include zero-point vibration state corrections. Based on these calculations free energies for each structure were estimated using the usual statistical mechanics formulae with temperatures relevant to the range of laboratory experimental conditions employed for the ODH reaction: 573, 673 and 773 K. A qualitative description of chemical bonding was also obtained based on the electron density shifts and atomic charges were analysed using the natural bonding orbital (NBO) [30,31] calculations as implemented in the GAUSSIAN 09 W package.

2.2. Model system

To represent the active site in this study, we have chosen the dimeric $H_4V_2O_7$ gas-phase model as illustrated in Fig. 1 [3,32]. Although this model simplifies the catalytic surface, we believe the calculated relative energies will provide insight about the most likely mechanistic steps that are followed and allows us to identify the intrinsic reactivity of oxygen species present. The selected model structure comprises two V(V)=*O* bonds, connected by a two-coordinated bridging O atom, V(V)-O-V(V), and the four H atoms are added to balance the total formal oxidation state charge of −4 on the four O atoms that would be coordinated onto the support and so ensure a metal oxidation state consistent with stoichiometric V_2O_5. Only the V(V)=*O* atom and the two-coordinated bridging O atom were considered for this study and all the atoms, including the four H atoms, were allowed to relax in calculations. The depicted optimized structure in Fig 1 is comparable with one the dimeric models suggested by Magg et al. [32]. The calculated bond length of the two V(V)=*O* bonds was 1.57 Å and that of the V(V)-O bonds comprising the two-coordinated bridging O atom was 1.77 Å. The percentage differences in the two calculated parameters are within 2% of the experimental solid-state structure [33]. The calculated IR ν_s(V=O) and ν_s(V-O-V) modes were 1106 and 765 cm^{-1}, with the respective percentage differences between the calculated vibrations and the

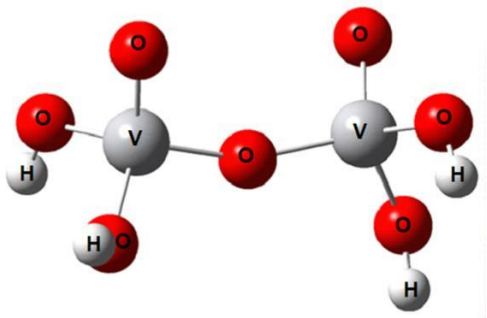

Fig. 1. $H_4V_2O_7$ model. UB3LYP/6–311+*G*(d,p) for H and O atoms, and ECP10MDF for V atom.

experimental values [32,34] being 5% and 1.5%, respectively. More detail is included as supplementary material.

2.3. Reaction scheme for the ODH conversion of n-hexane to 2-hexene

Fig. 2 depicts the proposed reaction scheme for ODH reaction of *n*-hexane using the example of the possible routes to 2-hexene catalysed by $H_4V_2O_7$. We concentrate on 1- and 2-hexene since there are no literature reports of the formation of 3-hexene in the product mixture, and we have also not identified it in our own experimental results [35].

We propose that β-H abstraction from the *n*-hexane chain (C_6H_{14}) by the V(V)=*O* atom in $H_4V_2O_7$ is the RDS. The resulting intermediate stabilises to a complex, $C_6H_{13}HOH_4V_2O_6$, with one of the V atoms reduced from the +5 to the +4 oxidation state. Three propagation pathways that may lead to 2-hexene are, (a) the gas-phase γ-H abstraction by O_2 to produce 2-hexene and a hydroperoxyl radical ($HO_2\bullet$) species, which can disproportionate in the termination step to produce water and oxygen, (b) the less thermodynamically stable surface γ-H abstraction by the adjacent V(V)=*O* in $HOH_4V_2O_6$ to produce 2-hexene and $HOHOH_4V_2O_5$ comprising two V(IV) centres, (c) the most thermodynamically stable surface γ-H abstraction by a V(V)=*O* on another $H_4V_2O_7$ active site to produce 2-hexene and $HOH_4V_2O_6$ containing one V(IV) centre. Although pathway (b) produces a less stable intermediate than pathway (c), the proximity of the $\bullet C_6H_{13}$ to the adjacent V(V)=*O* may render this pathway significant, more especially with low surface area of $H_4V_2O_7$ active sites. One of the two pathways that may regenerate the V(V) centre include intramolecular H-migration in $HOHOH_4V_2O_5$ (with two V(IV) centres) that is formed in propagation pathway (b) above, to produce H_2O, triplet-V(III) and V(V) centres in $H_4V_2O_6$. The other pathway involves intermolecular H-transfer between $HOH_4V_2O_6$ species (each with one V(IV) centre) formed in propagation pathway (c) above, to produce H_2O, V(V) centres, and $H_4V_2O_6$ comprising triplet-V(III) and V(V) centres. Lastly, the reoxidation of V (III) to V(V) may be achieved with interaction of surface O species with $H_4V_2O_6$ to produce $H_4V_2O_7$.

3. Results

3.1. Activation of n-hexane

We have investigated the radical mechanism in which there is C—H bond activation of *n*-hexane by vanadyl V(V)=*O* and bridging O atoms in $H_4V_2O_7$ laid out in Fig. 2 using the methodology described in Section 2.1. The energy profile for the initial β-H abstraction by either V(V)=*O* or bridging O are compared in Fig. 3 which shows Gibbs energy values calculated at 673 K. All other associated energies and temperatures are recorded in Table 1.

Several studies [20,21,36,37], have identified the C—H bond activation through β-H abstraction by the O atom in V(V)=*O* as the rate determining step (RDS). We calculated an activation barrier (TS_1 – Fig. 3) of $\Delta E^{\ddagger} = +32.7$ kcal mol^{-1} for a similar step, namely, the C—H bond activation in the interaction of C_6H_{14} and V(V)=*O* in $H_4V_2O_7$, leading to the formation of the intermediate complex, $C_6H_{13}HOH_4V_2O_6$ (Int_1), with $\Delta E = +31.6$ kcal mol^{-1}, relative to the reactants and only 1.1 kcal mol^{-1} below TS_1. The calculated $S(S+1)$ value for the RDS (TS_1) was 0.0556, confirming a singlet state, where S represents the total spin quantum number for the system. In our previous study with a single vanadyl complex [22], we calculated an activation barrier of $\Delta E^{\ddagger} = +27.4$ kcal mol^{-1} for H-abstraction by the V(V)=*O* in H_3VO_4 and $\Delta E^{\ddagger} = +42.4$ kcal mol^{-1} for H-abstraction by gas-phase O_2. Clearly, the present value falls between these two. The V(V)=*O* bond length in $H_4V_2O_7$ is elongated from 1.57 Å in the isolated unit to 1.70 Å in TS_1 and 1.76 Å in Int_1, and this is attributed to electron shift from a π-bonding orbital in V(V)=*O* to a *d*-orbital of V, resulting in reduction of V(V) to V(IV). Different authors [17,38,39] have experimentally characterised reduced V(IV) sites in both supported and unsupported vanadia catalysts. We also compared the above β-H abstraction step with that involving the bridging O in $H_4V_2O_7$. We calculated a higher barrier of $\Delta E^{\ddagger} = +43.9$ kcal mol^{-1} (TS_2 – Fig. 3), for C—H bond activation in C_6H_{14} by the bridging O atom in $H_4V_2O_7$, and the pathway leads to the formation of Int_2, which comprises the $\bullet C_6H_{13}$ radical intermediate adsorbed on to the V(V)=*O* atom. Although Int_2 ($\Delta E = +3.12$ kcal mol^{-1}) is thermodynamically more stable than Int_1 ($\Delta E = +31.6$ kcal mol^{-1}), the

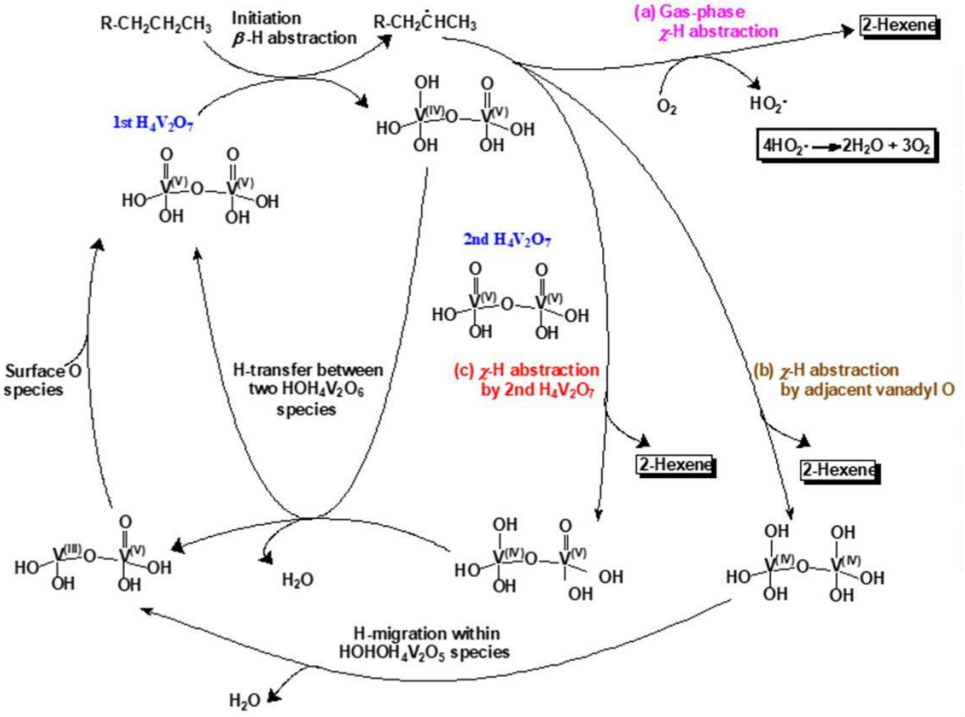

Fig. 2. Proposed reaction scheme, R-$CH_2CH_2CH_3$ with R-C_3H_7.

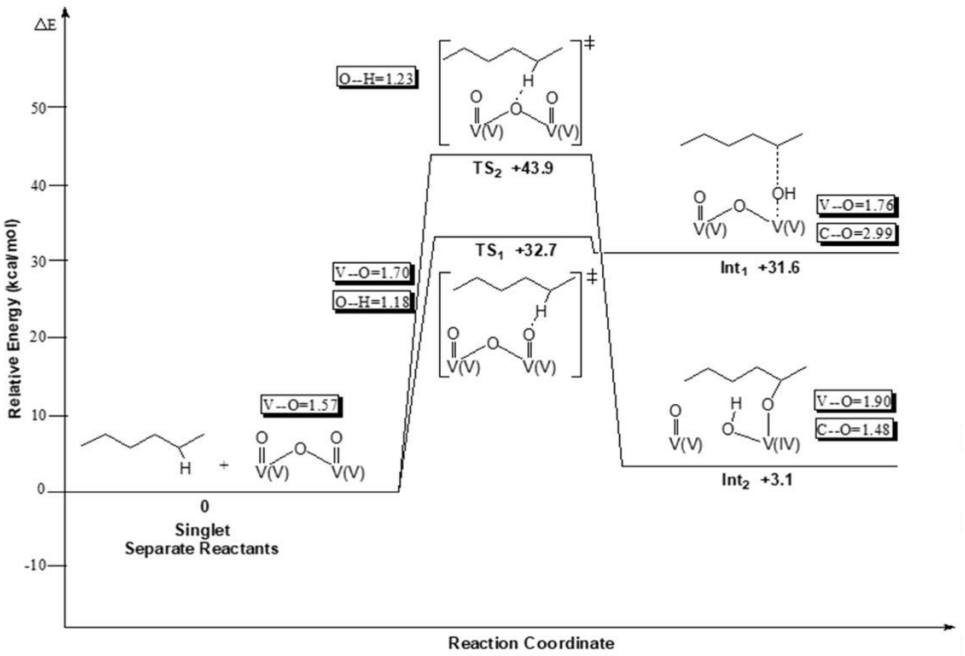

Fig. 3. Zero-point corrected relative (ΔE) reaction coordinate diagram for β-H activation of *n*-hexane over $H_4V_2O_7$ UB3LYP/6–311+*g*(d,p) for the C, O and H atoms, and Stuttgart ECP10MDF for the V atom. The indicated bond distances are in Angstrom units. Cartesian coordinates of all TS structures are provided as supplementary material.

pathway for its formation is likely to lead to side-reaction channels with production of carbon oxides and oxygenates, because of the formation of strong CO bonds [40]. Hui et al. [12] obtained similar results in their calculation of reaction barriers of the methylene C– H bond activation in ODH of propane over V_2O_5, with the V(V)=*O* and the bridging O being +27.3 and +30.4 kcal mol^{-1}, respectively. Our results show that the pathway for H-abstraction by the bridging O is not kinetically favoured with an energy barrier +11.2 kcal mol^{-1} higher than that for the V(V)=*O* species, and therefore we can conclude that the V(V)=*O* oxygen is likely to be the one involved in the C– H bond activation step of the mechanism.

We then explored the pathways, through Int_1, that are likely to lead to the formation of 1- and 2-hexene. Fig. 4 illustrates the energy diagram for the propagation steps to 2-hexene. All other results are presented in Table 1. The propagation step that involves γ-H abstraction in the $\bullet C_6H_{13}$ radical intermediate by the OH group in $HOH_4V_2O_6$ has an activation barrier of $\Delta E^{\ddagger}$ = +23.7 kcal mol^{-1} (TS_3 – Fig. 4, red-coloured pathway). This pathway leads to 2-hexene, H_2O and singlet $H_4V_2O_6$ (P_1) ΔE = +1.1 kcal mol^{-1}, with triplet P_1 being thermodynamically more stable, as expected, with ΔE = −27.2 kcal mol^{-1}, relative to reactants. The involvement of the bridging O in the similar propagation step was also examined, and a slightly lower barrier of $\Delta E^{\ddagger}$ = +22.9 kcal mol^{-1} was calculated. We then compared these energy barriers with that for γ-H abstraction in the $\bullet C_6H_{13}$ radical intermediate by the adjacent V(V)=*O* within Int_1 and obtained a lower value of $\Delta E^{\ddagger}$ = +9.1 kcal mol^{-1} (TS_4 – Fig. 4, blue-coloured pathway) and ΔE = +2.8 kcal mol^{-1}. Moreover, we calculated an even lower energy barrier of $\Delta E^{\ddagger}$ = +6.7 kcal mol^{-1} (TS_5 – Fig. 4, green-coloured pathway) and ΔE = −28.5 kcal mol^{-1}, for γ-H abstraction in the $\bullet C_6H_{13}$ radical intermediate by a V(V)=*O* on a different $H_4V_2O_7$ site. Examination of these results suggests that the propagation step that may lead to 2-hexene is less likely to involve γ-H abstraction by the OH group in $HOH_4V_2O_6$ and the bridging O, because these pathways are less kinetically favourable than the other two pathways, as also partly determined in our previous results of gas-phase activation of *n*-hexane over isolated H_3VO_4 species [22]. Therefore, either γ-H abstraction by the adjacent V(V)=*O* within Int_1 ($\Delta E^{\ddagger}$ = +9.1 kcal mol^{-1}) or γ-H abstraction by a V(V)=*O* on a different $H_4V_2O_7$ site ($\Delta E^{\ddagger}$ = +6.7 kcal mol^{-1}) are likely to be possible pathways to produce 2-hexene. The preferred pathway is likely to depend on proximity of the $\bullet C_6H_{13}$ radical intermediate to either the adjacent V(V)=*O* within Int_1 or the V(V)=*O* species on a different $H_4V_2O_7$ site. However, as stated earlier, chemisorption of the $\bullet C_6H_{13}$ radical intermediate to surface O atoms may lead to side reactions, with high barriers for releasing 2-hexene and thereby enabling side-reaction channels, such as complete oxidation to undesired carbon oxides and oxygenates [40]. In our previous studies on gas-phase ODH of *n*-hexane over isolated H_3VO_4 [22], we calculated a barrierless reaction step for this process with $\Delta E^{\ddagger}$ = −4.2 kcal mol^{-1}, indicating a stable intermediate for the chemisorption of the hexyl radical on to the V(V)=*O* species. This observation may explain why low yields of less than 20% for 1- and 2-hexene are obtained in our laboratory experiments. Chemisorption of alkyl radicals has also been reported on selective oxidation of propane over V_2O_5 and V_2O_5/TiO_2 by Alexopoulos et al. [41], who concluded that propene formation via an adsorbed propoxide intermediate is less favourable than propene formation directly from the propyl radical without chemisorption.

Both propagation pathways (through TS_4 and TS_5) that are likely to produce the hexenes may lead to the accumulation of the OH groups on the surface. From the P_2 and P_5 fragment ($HOHOH_4V_2O_5$) that is likely to be produced through TS_4, we then investigated the intramolecular H-migration pathway from one OH group to the other within the fragment. We calculated a barrierless pathway with the initial complex intermediate (ΔE = −21.5 kcal mol^{-1}) that stabilizes to triplet-V(III) Int $_3$ with ΔE = −35.0 kcal mol^{-1} (Fig. 5, pathway A). Clearly, this concerted mechanistic step is associated with the formation of a new O– H bond to produce H_2O, and the scission of the O– H and V-O bonds. Furthermore, from the P_3 and P_6 fragment ($HOH_4V_2O_6$), we calculated intermolecular H-transfer between two fragments that are likely to be produced through TS_5. We obtained an energy barrier of $\Delta E^{\ddagger}$ = +3.3 (TS_9 – Fig. 5, pathway B) and ΔE = −18.3 kcal mol^{-1}, relative to reactants, for the formation of H_2O, regenerated $H_4V_2O_7$ and $H_4V_2O_6$ (Int_4) that also comprises the triplet V(III)-O-V(V) fragment. From the calculated energies ($\Delta E^{\ddagger}$ and ΔE) of the two reaction pathways in Fig. 5, we can conclude that both are kinetically and thermodynamically favourable, in agreement with

Table 1
Relative Energies (ΔE) and Gibbs Energies (ΔG) for the reaction of *n*-hexane with $H_4V_2O_7$ to produce 1- and 2-hexene[a]. UB3LYP/6–311+*g*(d,p) for the C, O and H atoms, and Stuttgart ECP10MDF for the V atom. Cartesian coordinates of all TS structures are provided as supplementary material.

Reaction Pathway	ΔE	ΔG		
		573	673	773
Initiation				
s-C_6H_{14} + $H_4V_2O_7$	0	0	0	0
s-C_6H_{14} + $H_4V_2O_7$ (TS_1) – V (V)=*O*	+32.7	+49.3	+52.5	+55.6
s-TS_1→C_6H_{13}–$HOH_4V_2O_6$ (Int_1)	+31.6 (-1.1)	+42.3 (-7.0)	+44.4 (-8.1)	+46.5 (-9.1)
s-C_6H_{14}–$H_4V_2O_7$ (TS_2) – bridging O	+43.9	+62.7	+67.3	+72.7
s-TS_1→C_6H_{13}–$HOH_4V_2O_6$ (Int_2)	+3.1 (-40.8)	+26.0 (-36.7)	+30.2 (-37.1)	+34.3 (-38.3)
Propagation from HOH_4V_2O				
s-C_6H_{13}+HOH_4V_2O [6]	0	0	0	0
s-C_6H_{13}–$HOH_4V_2O_6$(TS_3)	+23.7	+43.2	+55.0	+53.6
s-TS_3→2-**Hexene** +$H_4V_2O_6$ + H_2O (P)	+1.1 (-22.6)	+18.6 (-24.6)	+23.5 (-31.5)	+25.3 (-28.3)
t-2-**Hexene** + $H_4V_2O_6$ + H_2O (P_1)	-27.2	-10.6	-6.9	-4.07
s-C_6H_{13}–$HOH_4V_2O_6$ (TS_6)	+24.4	+48.0	+56.7	+60.7
s-TS_6→1-**Hexene** +$H_4V_2O_6$ + H_2O (P_4)	-13.1 (-37.5)	+8.0 (-40.0)	+7.9 (-48.8)	+16.3 (-44.4)
t-1-**Hexene** + $H_4V_2O_6$ + H_2O (P_4)	-24.8	-6.8	-5.9	-2.4
Propagation from adjacent V (V)=*O*				
s-C_6H_{13} + $HOH_4V_2O_6$	0	0	0	0
s-C_6H_{13}–$HOH_4V_2O_6$ (TS_4)	+9.1	+29.3	+33.4	+36.8
s-TS_4→2-Hexene + $HOHOH_4V_2O_5$ (P_2)	+2.8 (-6.3)	-7.9 (-37.2)	+10.1 (-23.3)	-0.8 (-37.6)
s-C_6H_{13}–$HOH_4V_2O_6$ (TS_7)	+9.6	+28.6	+33.1	+35.8
s-TS_7→1-Hexene + $HOHOH_4V_2O_5$ (P_5)	-23.0 (-32.6)	-4.0 (-32.6)	+1.0 (-32.1)	+3.1 (-32.7)
Propagation from separate V (V)=*O* site				
d-C_6H_{13} + $H_4V_2O_7$	0	0	0	0
d-C_6H_{13}–$H_4V_2O_7$ (TS_5)	+6.7	+25.3	+28.5	+32.3
d-TS_5→2-Hexene +$HOH_4V_2O_6$ (P_3)	-28.5 (-35.2)	-11.9 (-37.2)	-8.8 (-37.3)	-5.6 (-37.9)
d-C_6H_{13}–$H_4V_2O_7$ (TS_8)	+7.2	+25.3	+29.4	+32.0
d-TS_8→1-Hexene +$HOH_4V_2O_6$ (P_6)	-25.3 (-32.5)	-9.8 (-35.1)	-5.5 (-34.9)	-3.9 (-35.9)
H-migration within $HOHOH_4V_2O_5$				
s-$HOHOH_4V_2O$	0	0	0	0
s-$H_4V_2O_6$ + H_2O (Int_3)	-23.3	-11.4	-21.4	-9.8
t-$H_4V_2O_6$ + H_2O (Int_3)	-35.0	-24.3	-34.5	-23.1
H-transfer between two HOH_4V_2O				
s-$HOH_4V_2O_6$ + $HOH_4V_2O_6$	0	0	0	0
s-$HOH_4V_2O_6$–$HOH_4V_2O_6$ (TS_9)	+3.3	+28.5	+35.0	+37.8
s-TS_9→$H_4V_2O_7$ + $H_4V_2O_6$ + H_2O (Int_4)	-6.2 (-9.5)	+19.6 (-8.9)	+24.3 (-10.7)	+29.1 (-8.7)
t-$H_4V_2O_7$ + $H_4V_2O_6$ + H_2O (Int_4)	-18.3	+6.4	+10.9	+15.5
Reoxidation of *t*-$H_4V_2O_6$ by surface O				
surface O + $H_4V_2O_6$	0	0	0	0
s-$H_4V_2O_7$ (P_7)	-253.3	-231.5	-227.5	-223.5

[a] ΔE and ΔG are zero-point corrected electronic energy and Gibbs energy at standard pressure, relative to separate reactants respectively, in kcal mol^{-1}. The energies in parentheses are for the indicated reaction pathways. The temperature is in K and prefixes *s*-,*d*- and *t*- indicate singlet, doublet, and triplet states, respectively.

previous literature [12,42].

Reoxidation of triplet V(III)-O-V(V) to V(V)-O-V(V) is likely to proceed via a Mars-van Krevelen mechanism. Our results indicate that the adsorption of surface O species onto the triplet-V(III) centre is a barrierless process with $H_4V_2O_7$ stabilization of ΔE = -253.3 kcal mol^{-1} (Table 1). As reported in our previous studies, the involvement of gas-phase O_2 is likely to be limited to propagation steps that may lead to the hexenes, provided the $\bullet C_6H_{13}$ radical intermediate is released to the gas-phase rather than being chemisorbed onto the surface O [22,43]. The resulting hydroperoxyl radicals ($HO_2\bullet$) from H-abstraction by O_2 are likely to disproportionate to produce H_2O and regenerate O_2.

It is important to add that periodic-DFT calculations on this system are likely to improve the quality of the calculated energetics because of better representation of the catalytic solid surface.

3.2. Temperature effects

All the reaction pathways were modelled using the laboratory experimental conditions of 573, 673 and 773 K. Table 1 displays the calculated Gibbs energies of activation ($\Delta G^{\ddagger}$) and Gibbs energy changes (ΔG) for all the reaction pathways at the three indicated temperatures.

Transition state theory was used to calculate the rate constants (k) per active site over the three temperatures for the RDS. The $\Delta G^{\ddagger}$ values increase as the temperature increases from 573 to 673 and 773 K. From the $\Delta G^{\ddagger}$ values we calculated the corresponding k values and obtained the following results, $k(573) = 1.87 \times 10^{-6}$ s^{-1}, $k(673) = 1.25 \times 10^{-4}$ s^{-1} and $k(773) = 3.06 \times 10^{-3}$ s^{-1}. The calculated $k(773)$ per active site is approximately three orders of magnitude greater than that at 573 K and one order of magnitude greater than that at 673 K. The calculated ΔG values for the RDS are +42.3, +44.4 and +46.5 kcal mol^{-1} at 573, 673 and 773 K for the formation of Int_1, respectively. From the attached supplementary material, the lowest enthalpy (ΔH = +29.7 kcal mol^{-1}) and entropy ($T\Delta S$ = -12.6 kcal mol^{-1}) contributions were calculated at 573 K and highest values were obtained at 773 K (ΔH = +30.9 and $T\Delta S$ = -15.6 kcal mol^{-1}). The ΔH contributions are the dominant factors to the ΔG values at all temperatures and are approximately 2.5 times the magnitude values of $T\Delta S$. Clearly, 573 K is the thermodynamically more favourable temperature for the formation of Int_1. It is important to mention that similar trends in terms of the calculated rate constants per active site, ΔH, $T\Delta S$ and ΔG values were also observed in our previous study of the same reaction over H_3VO_4 [22].

For other reaction pathways, we calculated negative ΔG values for the barrierless H-migration pathway at all temperatures, whereas a low positive values of $\Delta G^{\ddagger}$, and ΔG values which increase with temperature, were obtained for the H-transfer step (TS_9). This shows that the intramolecular H-migration pathway is kinetically and thermodynamically favourable at all temperatures, and the intermolecular H-transfer pathway is kinetically more favourable at 773 K and thermodynamically favourable at 573 K. The pathway for the reoxidation of triplet V(III) to V(V) is a barrierless process that indicate that this step is kinetically and thermodynamically favourable over the temperature range.

Hence, the formation of 1- and 2-hexene from activation of *n*-hexane by β-H abstraction with surface V(V)=*O* oxygen ($H_4V_2O_7$) followed by the second H-abstraction from either a different V(V)=*O* oxygen ($H_4V_2O_7$) or from gas-phase O_2, is likely to be more kinetically more favourable at 773 K and thermodynamically more favourable at 573 K.

3.3. Natural bond orbital analyses

The qualitative description of the reaction steps was conducted through NBO calculations [30,31] at the UB3LYP/6–311+*G*(d,p) level on the TSs of the RDS and propagation steps leading to the formation of 2-hexene. The TSs and the frontier orbitals represented by donor and acceptor orbitals are illustrated in Fig. 6. Table 2 lists the selected TSs, the atomic charges of the interacting atoms, the frontier orbitals, and the orbital stabilization energies.

The singly occupied molecular orbital (SOMO) for the activation of *n*-hexane through the RDS (TS1) comprises O of *s*(7.5%) *p*(92.5%) nonbonding type character. The LUMO is made up of the C of *s*(10.8%) *p* (65.0%) and H of *s*(24.2%) antibonding type character. The transfer of electron density between the two orbitals is associated with the

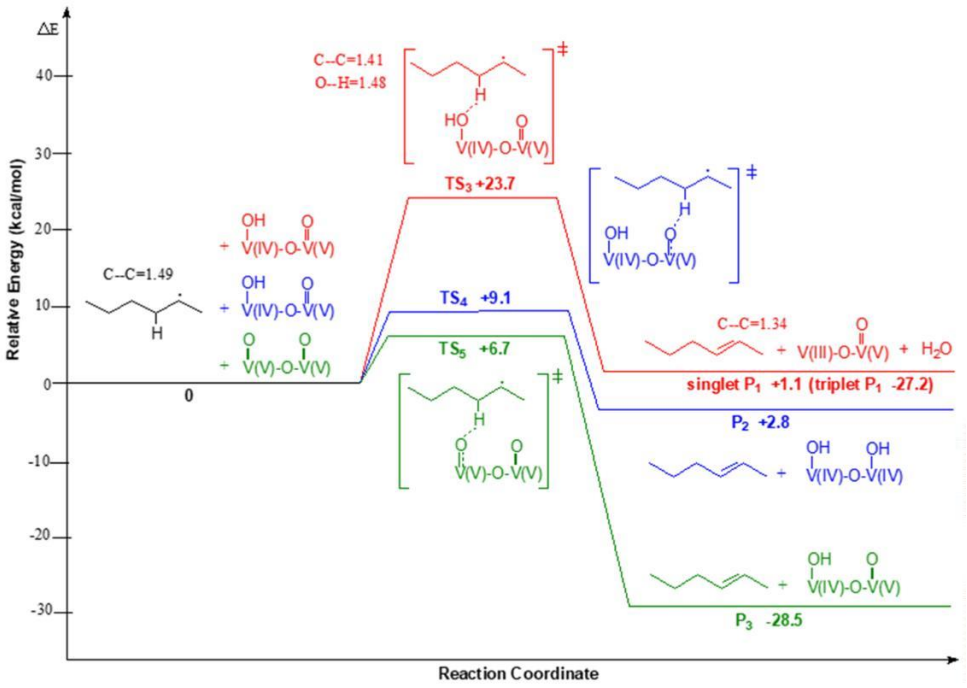

Fig. 4. Zero-point corrected relative energy (ΔE) reaction coordinate diagram for propagation pathways for the formation of 2-hexene. The red colour indicates the pathway for γ-H abstraction from C_6H_{13} by the OH group in Inti. The blue colour represents the pathway for y-H abstraction from an adjacent V(V)-O in Int_1 and the green colour displays the most kinetically and thermodynamically favourable pathway for γ -H abstraction from a different V(V)-O site. UB3LYP/6–311+*g*(d,p) for the C, O and H atoms, and Stuttgart ECP10MDF for the V atom. The indicated bond distances are in Angstrom units. Cartesian coordinates of all TS structures are provided as supplementary material.

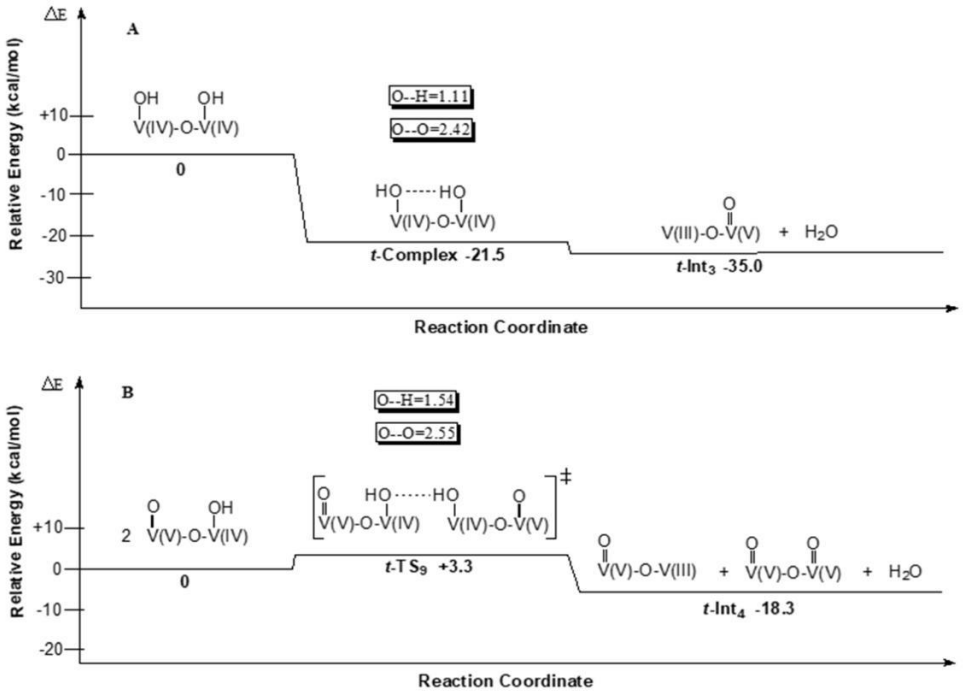

Fig. 5. Zero-point corrected relative energy (ΔE) reaction coordinate diagrams for intramolecular H- migration in $HOHOH_4V_2O_5$ to produce H_2O and the triplet V(III)-O-V(V) species (pathway A) and intermolecular H-transfer between two $HOH_4V_2O_6$ units to produce H_2O, triplet V(III)-O-V(V) and regenerated V(V)-O-V (V) species (pathway B). UB3LYP/6–311+*g*(d, p) for the C, O and H atoms, and Stuttgart ECP10MDF for the V atom. The indicated bond distances are in Angstrom units. The t- prefix indicates the triplet state. Cartesian coordinates of all TS structures are provided as supplementary material.

stabilization energy of +164.1 kcal mol^{-1}. Our results indicate that this value may be attributed to strong interaction between the aligned HOMO and LUMO orbitals which facilitate the flow of electron density leading to large and remote delocalization within the system. The calculated atomic charges of the interacting atoms are O (-0.577), H (+0.362) and C (-0.239), indicating a stronger attraction of the positive H atom by the negative O atom. It may be mentioned that the calculated atomic charges of H and C in *n*-hexane are lower at +0.135 and-0.180, respectively, and the charges increase in the TS in line with a shift of some electron density from O to C and H during bond scission. The donor and acceptor orbitals describing the propagation pathway barriers for the formation of 2-hexene (TS_4) through H-abstraction by an adjacent V (V)=*O* are the O *s*(80.1%) *p*(19.9%) nonbonding hybrid and the V *s* (13.1%) *p*(81.0%) *d*(5.9%) antibonding hybrid, respectively. The calculated stabilization energy is +39.2 kcal mol^{-1}. The distribution of atomic charges on interacting atoms are C (-0.506), H (+0.317) and O (-0.460). An alternative pathway that may lead to 2-hexene is H-abstraction by a different V(V)=*O* site (TS_5), and the associated donor orbital is the O *s*(80.9%) *p*(19.1%) nonbonding hybrid, and the acceptor orbital is the V *s*(13.0%) *p*(81.2%) *d*(5.8%) antibonding hybrid, with stabilization energy of +41.6 kcal mol^{-1}. The lower stabilization energies for TS4 and TS5 as compared to TS1 may be attributed to lower

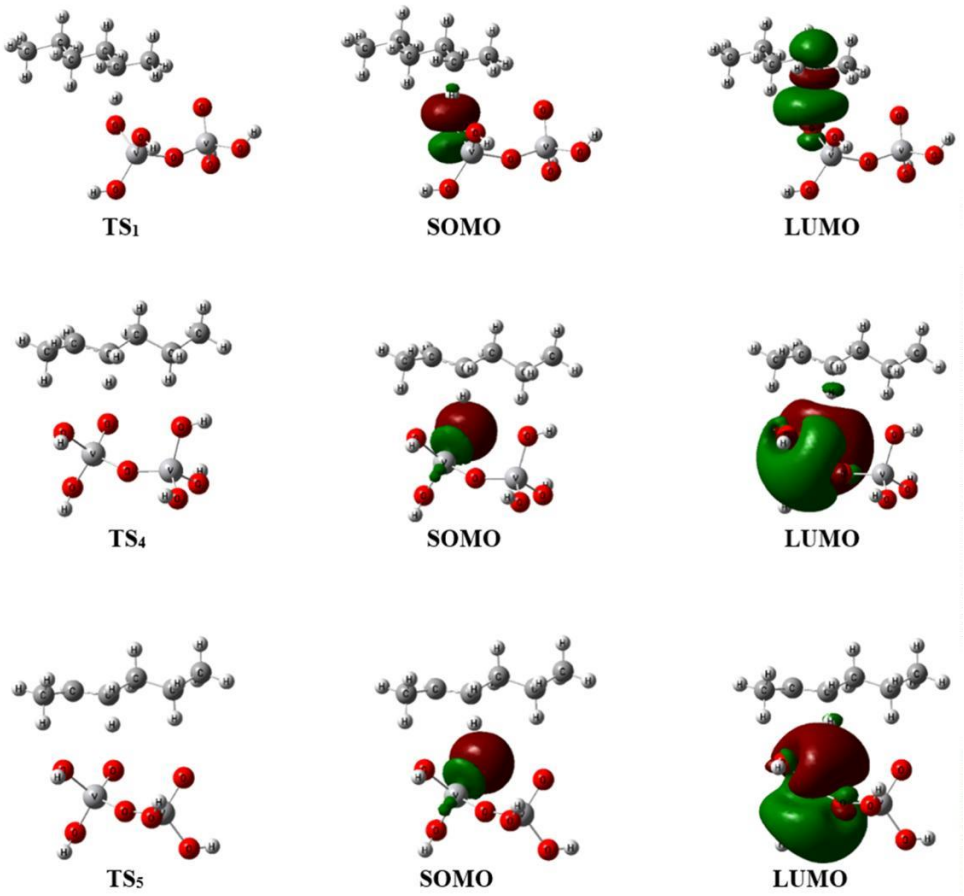

Fig. 6. Selected TS structures and the NBO calculated frontier orbitals for the likely mechanistic pathways for the formation of 2-hexene. The orbital lobes are orientated for better clarity in each case and correspond to the reaction coordinate. UB3LYP/6–311+*g*(d,p) for all the atoms. Cartesian coordinates of all TS structures are provided as supplementary material.

Table 2
Selected NBO atomic charges, SOMO and LUMO orbital types, and orbital energies for the TS structures of the *n*-hexane to 2-hexene pathway. UB3LYP/6-311+g(d,p) for all the atoms. Cartesian coordinates of all TS structures are provided as supplementary material.

TS	Atomic charges on interacting atoms	SOMO type (donor)	LUMO type (acceptor)	Largest Orbital Stabilization Energy (kcal mol^{-1})
1	C = –0.239	O *s*(7.5%) *p* (92.5%)	C *s*(10.8%) *p* (65.0%)	+164.1
	H = +0.362	nonbonding	H *s*(24.2%)	
	O = –0.577	hybrid	antibonding	
4	C = –0.506	O *s*(80.1%) *p* (19.9%)	V *s*(13.1%) *p* (81.0%)	+39.2
	H = +0.317	nonbonding	*d*(5.9%) antibonding	
	O = –0.460	hybrid	hybrid	
5	C = –0.507	O *s*(80.9%) *p* (19.1%)	V *s*(13.1%) *p* (81.1%)	+41.6
	H = +0.310	nonbonding	*d*(5.8%) antibonding	
	O = –0.432	hybrid	hybrid	

delocalization of electron density within the system. The atomic charges on interacting atoms follow a similar trend, with C (-0.507), H (+0.310) and O (-0.432).

4. Conclusions

The activation of *n*-hexane over $H_4V_2O_7$ has been modelled using DFT methods at the UB3LYP level, with the 6–311+*G*(d,p) basis set for C, O and H atoms, and ECP10MDF for the V atom. The following mechanistic pathways are proposed for the formation of 1- and 2-hexene,

(i) Initiation: $C_6H_{14} + H_4V_2O_7 = C_6H_{13} + HOH_4V_2O_6$

The interaction of *n*-hexane with $H_4V_2O_7$ leads to *β*-H abstraction by V(V)=*O* in $H_4V_2O_7$ to produce the $\bullet C_6H_{13}$ + $HOH_4V_2O_6$ complex intermediate. This is the RDS with a barrier height of $\Delta E^{\ddagger} = +32.7$ kcal mol^{-1} (TS$_1$). This value is higher than that obtained in our previous work on gas-phase ODH by V(V)=*O* in H_3VO_4 ($\Delta E^{\ddagger} = +27.4$ kcal mol^{-1}). The complex intermediate (Int$_1$) stabilizes with $\Delta E = +31.6$ kcal mol^{-1}, relative to the reactants (Fig. 3 and Table 1).

(ii) Propagation on adjacent V(V)=*O*: $C_6H_{13} + HOH_4V_2O_6 = C_6H_{12} + HOHOH_4V_2O_5$

γ-H abstraction occurs through V(V)=*O* that is adjacent to the V(IV)-OH unit of the $HOH_4V_2O_6$ fragment in Int$_1$. The calculated energy barrier is $\Delta E^{\ddagger} = +9.1$ kcal mol^{-1} (TS$_4$) and the produced P$_2$(2-hexene) complex stabilizes to $\Delta E = +2.8$ kcal mol^{-1}, relative to reactants (Fig. 4 and Table 1).

(iii) Propagation on different V(V)=*O*: $C_6H_{13} + H_4V_2O_7 = C_6H_{12} + HOH_4V_2O_6$

The propagation pathway described in (ii) above is likely to compete with the *γ*-H abstraction by V(V)=*O* on a different site. This step has $\Delta E^{\ddagger}$

$= +6.7$ kcal mol^{-1} (TS_5) and the P_3 (2-hexene) complex stabilize to $\Delta E = -28.5$ kcal mol^{-1}, relative to reactants. The pathway that is likely to occur between (ii) and (iii) may depend on proximity of the $\bullet C_6H_{13}$ radical intermediate to either the adjacent V(V)=*O* or the V(V)=*O* on a

(iv) Intramolecular H-migration: $HOHOH_4V_2O_5 = H_4V_2O_6 + H_2O$

The propagation pathway described in (ii) above leads to the formation of two OH groups and two V(IV) centres in $HOHOH_4V_2O_5$. The pathway for the migration of the H atom from one OH group to the other is likely to be a barrierless step with the complex intermediate (Int_3) containing a triplet-V(III) centre, which stabilizes to $\Delta E = -35.0$ kcal mol^{-1} (Fig. 5A and Table 1).

(v) Intermolecular H-transfer: $HOH_4V_2O_6 + HOH_4V_2O_6 = H_4V_2O_7 + H_4V_2O_6 + H_2O$

Similarly, the propagation pathway (iii) described above is likely to lead to the formation of an OH group and one V(IV) centre in $HOH_4V_2O_6$. Therefore H-transfer may occur between two $HOH_4V_2O_6$ units, and we calculated a barrier of $\Delta E^{\ddagger} = +3.3$ kcal mol^{-1} (TS_4), with the complex intermediate (Int_4) comprising separate triplet-V(III) and V(V) centres stabilizing to $\Delta E = -18.3$ kcal mol^{-1} (Fig. 5B and Table 1).

(vi) Reoxidation and Termination: $H_4V_2O_6 + \text{"surface O"} = H_4V_2O_7$

The generated V(III) complex ($H_4V_2O_6$) from pathways (iv) and (v) above, is likely to undergo reoxidation by surface O species to produce the initial V(V) centres ($H_4V_2O_7$). Our results indicate that this step is barrierless with $\Delta E = -253.3$ kcal mol^{-1} for the formation of the initial V(V) centre ($H_4V_2O_7$) (Table 1).

From our calculations (Table 1) we may conclude that the selectivity towards 2-hexene is likely to be higher than that for 1-hexene under the specified conditions. The low yields (<20%) towards alkenes that are obtained in our laboratory experiments may be explained by the calculated intermediates that form strong C–O bonds with branching toward total oxidation products.

CRediT authorship contribution statement

Nkululeko E. Damoyi: Conceptualization, Methodology, Software, Data curation, Writing – original draft, Visualization, Investigation, Software, Validation, Writing – review & editing. **Holger B. Friedrich:** Conceptualization, Methodology, Software, Supervision, Writing – review & editing. **Gert H. Kruger:** Conceptualization, Methodology, Software, Supervision, Writing – review & editing. **David J. Willock:** Conceptualization, Methodology, Software, Supervision, Software, Validation, Writing – review & editing.

Declaration of Competing Interest

The authors declare that they have no known competing financial interests or personal relationships that could have appeared to influence the work reported in this paper.

Data availability

Data will be made available on request.

Acknowledgments

This work was supported by the NRF, SASOL LTD and Johnsson Matthey. We would like to thank the Centre for High Performance Computing (CHPC) in Cape Town, South Africa, for providing the computational resources necessary to conduct this work.

References

[1] P. Eisele, R. Killpack, Ullmann's Encyclopedia of Industrial Chemistry, Wiley-VCH, 2000.
[2] T. Blasco, J.M. López Nieto, Oxidative dehydrogenation of short chain alkanes on supported vanadium oxide catalysts, Appl. Catal. A 157 (1997) 117–142.
[3] B. Beck, M. Harth, N.G. Hamilton, C. Carrero, J. Uhlrich, A. Trunschke, S. Shaikhutdinov, H. Schubert, H.J. Freund, R. Schlögl, J. Sauer, R. Schomäcker, Partial oxidation of ethanol on vanadia catalysts on supporting oxides with different redox properties compared to propane, J. Catal. 296 (2012) 120–131.
[4] A. Corma, J.M. López Nieto, N. Paredes, Influence of the preparation methods of V-Mg-O catalysts on their catalytic properties for the oxidative dehydrogenation of propane, J. Catal. 144 (1993) 425–438.
[5] M.A. Chaar, D. Patel, H.H. Kung, Selective oxidative dehydrogenation of propane over V-Mg-O catalysts, J. Catal. 109 (1988) 463–467.
[6] F.D. Hardcastle, I.E. Wachs, Raman spectroscopy of chromium oxide supported on Al_2O_3, $TiO_2$and SiO_2: a comparative study, J. Mol. Catal. 46 (1988) 173–186.
[7] I.E. Wachs, B.M. Wechuysen, Structure and reactivity of surface vanadium oxide species on oxide support, Appl. Catal. A 157 (1997) 67–90.
[8] P. Mars, D.W. van Krevelen, Oxidations carried out by means of vanadium oxide catalysts, Chem. Eng. Sci. 3 (1954) 41–59.
[9] D. Yun, Y. Wang, J.E. Herrera, Ethanol partial oxidation over VOx/TiO_2 catalysts: the role of titania surface oxygen on vanadia reoxidation in the mars–van Krevelen mechanism, ACS Catal. 8 (2018) 4681–4693.
[10] A. Goodrow, A.T. Bell, A theoretical investigation of the selective oxidation of methanol to formaldehyde on isolated vanadate species supported on titania, J. Phys. Chem. C 112 (2008) 13204–13214.
[11] K. Chen, A. Khodakov, J. Yang, A.T. Bell, E. Iglesia, Isotopic tracer and kinetic studies of oxidative dehydrogenation pathways on vanadium oxide catalysts, J. Catal. 186 (1999) 325–333.
[12] F. Hui, L. Zhi-Pan, L. Zhen-Hua, W. Wen-Ning, F. Kang-Nian, Periodic density functional theory study of propane oxidative dehydrogenation over V_2O_5(001) surface, J. Am. Chem. Soc. 128 (2006) 11114–11123.
[13] A.M. Prakash, M. Hartmann, Z. Zhu, L. Kevan, Incorporation of transition metal ions into MeAPO/MeAPSO molecular sieves, J. Phys. Chem. B 104 (2000) 1610–1616.
[14] K.D. Chen, A.T. Bell, E. Iglesia, The relationship between the electronic and redox properties of dispersed metal oxides and their turnover rates in oxidative dehydrogenation reactions, J. Catal. 209 (2002) 35–42.
[15] S.T. Oyama, Adsorbate bonding and the selection of partial and total oxidation pathways, J. Catal. 128 (1991) 210–217.
[16] K. Mori, A. Miyamoto, Y. Murakami, Catalytic reactions on well-characterized vanadium oxide catalysts. 4. Oxidation of butane, J. Phys. Chem. 89 (1985) 4265–4269.
[17] J.G. Eon, R. Olier, J.C. Volta, Oxidative dehydrogenation of propane on γ-Al_2O_3supported vanadium oxides, J. Catal. 145 (1994) 318–326.
[18] R. Ramirez, B. Casal, L. Utrera, E. Ruiz-Hitzky, Oxygen reactivity in vanadium pentoxide: electronic structure and infrared spectroscopy studies, J. Phys. Chem. 94 (1990) 8960–8965.
[19] A. Fahmi, C. Minot, A theoretical investigation of water adsorption on titanium dioxide surfaces, Surf. Sci. 304 (1994) 343–359.
[20] X. Rozanska, R. Fortrie, J. Sauer, Oxidative dehydrogenation of propane by monomeric vanadium oxide sites on silica support, J. Phys. Chem. C 111 (2007) 6041–6050.
[21] M. Cheng, K. Chenoweth, J. Oxgaard, A. van Duin, W. Goddard, Single-site vanadyl activation, functionalization, and reoxidation reaction mechanism for propane oxidative dehydrogenation on the cubic V_4O_{10} cluster, J. Phys.Chem. C 111 (2007) 5115–5127.
[22] N.E. Damoyi, H.B. Friedrich, H.G. Kruger, D. Willock, A DFT Study of the ODH of *n*-hexane over isolated H_3VO_4, J. Mol. Catal. 452 (2018) 83–92.
[23] M.J. Frisch, G.W. Trucks, H.B. Schlegel, G.E. Scuseria, M.A. Robb, J.R. Cheeseman, G. Scalmani, V. Barone, B. Mennucci, G.A. Petersson, H. Nakatsuji, M. Caricato, X. Li, H.P. Hratchian, A.F. Izmaylov, J. Bloino, G. Zheng, J.L. Sonnenberg, M. Hada, M. Ehara, K. Toyota, R. Fukuda, J. Hasegawa, M. Ishida, T. Nakajima, Y. Honda, O. Kitao, H. Nakai, T. Vreven, J. Montgomery, J. A, J.E. Peralta, F. Ogliaro, M. Bearpark, J.J. Heyd, E. Brothers, K.N. Kudin, V.N. Staroverov, R. Kobayashi, J. Normand, K. Raghavachari, A. Rendell, J.C. Burant, S.S. Iyengar, J. Tomasi, M. Cossi, N. Rega, N.J. Millam, M. Klene, J.E. Knox, J.B. Cross, V. Bakken, C. Adamo, J. Jaramillo, R. Gomperts, R.E. Stratmann, O. Yazyev, A.J. Austin, R. Cammi, C. Pomelli, J.W. Ochterski, R.L. Martin, K. Morokuma, V.G. Zakrzewski, G.A. Voth, P. Salvador, J.J. Dannenberg, S. Dapprich, A.D. Daniels, O. Farkas, J. B. Foresman, J.V. Ortiz, J. Cioslowski, D.J. Fox, Gaussian 09, Revision B.01, Gaussian, Inc., Wallingford, 2010.
[24] A.D. Becke, Density functional thermochemistry III – The role of exact exchange, J. Chem. Phys. 98 (1993) 5648–5652.

[25] C. Lee, W. Yang, R.G. Parr, Development of the Colle-Salvetti correlation energy formula into a functional of the electron density, Phys. Rev. B Condens. Matter 37 (1988) 785–789.
[26] M. Dolg, U. Wedig, H. Stoll, H. Preuss, Energy-adjusted ab initio pseudopotentials for the first-row transition elements, J. Chem. Phys. 86 (1987) 866–872.
[27] J.M.L. Martin, A. Sundermann, Correlation consistent valence basis sets for use with the Stuttgart-Dresden-Bonn relativistic effective core potentials: the atoms Ga-Kr and In-Xe, J. Chem. Phys. 114 (2001) 3408–3420.
[28] C. Gonzales, H.B. Schlegel, An improved algorithm for reaction path following, J. Chem. Phys. 90 (1989) 2154–2161.
[29] C. Gonzales, H.B. Schlegel, Reaction path following in mass-weighted internal coordinates, J. Phys. Chem. 94 (1990) 5523–5527.
[30] J.E. Carpenter, F. Weinhold, Analysis of the geometry of the hydroxymethyl radical by the "different hybrids for different spins" natural bond orbital procedure, J. Mol. Struct. THEOCHEM 169 (1988) 41–62.
[31] J.E. Carpenter, F. Weinhold, R. Naaman, Z. Vager, The natural bond orbital Lewis structure concept for molecules, radicals, and radical ions. The Structure of Small Molecules and Ions, Plenum, N.Y., 1988, pp. 227–236.
[32] N. Magg, B. Immaraporn, J.B. Giorgi, T. Schroeder, M. Bäumer, J. Döbler, Z. Wu, E. Kondratenko, M. Cherian, M. Baerns, P.C. Stair, J. Sauer, H.J. Freund, Vibrational spectra of alumina- and silica-supported vanadia revisited: an experimental and theoretical model catalyst study, J. Catal. 226 (2004) 88–100.
[33] I.D. Brown, D. Altermatt, Bond-valence parameters obtained from a systematic analysis of the Inorganic crystal structure database, Acta. Crystallogr. B Struct. Sci. 4 (1985) 244–247, 41.
[34] N. Magg, J.B. Giorgi, T. Schroeder, M. Bäumer, H.-J. Freund, Model Catalyst Studies on Vanadia Particles Deposited onto a Thin-Film Alumina Support. Structural Characterization, J. Phys. Chem. B 34 (2002) 8756–8761, 106.
[35] J. Chetty, S. Singh, H.B. Friedrich, The oxidative aromatization of *n*-hexane over VMgO catalysts, Reac. Kinet. Mech. Cat. 120 (2017) 307–321.
[36] K.D. Chen, A.T. Bell, E. Iglesia, Kinetic isotopic effects in oxidative dehydrogenation of propane on vanadium oxide catalysts, J. Catal. 192 (2000) 197–203.
[37] M.D. Argyle, K. Chen, E. Iglesia, A.T. Bell, Effect of catalyst structure on oxidative dehydrogenation of ethane and propane on alumina-supported vanadia, J. Catal. 208 (2002) 139–149.
[38] K. Tamara, S. Yoshida, S. Ishida, H. Kakioka, Spectroscopic studies of catalysis by vanadium pentoxide, Bull. Chem. Soc. Jpn. 41 (1968) 2840–2845.
[39] K. Devriendt, H. Poelman, L. Fiermans, G. Creten, G.F. Froment, Angular resolved XPS applied to V_2O_5-based catalysts, Surf. Sci. 352–354 (1996) 750–754.
[40] M.D. Argyle, K. Chen, C. Resini, C. Krebs, A.T. Bell, E. Iglesia, Extent of reduction of vanadium oxides during catalytic oxidation of alkanes measured by *in-situ* UV–Visible spectroscopy, J. Phys. Chem. B 108 (2004) 2345–2353.
[41] K. Alexopoulos, M. Reyniers, G.B. Marin, Reaction path analysis of propane selective oxidation over $V_2O_5$and V_2O_5/TiO_2, J. Catal. 289 (2012) 127–139.
[42] L. Cheng, G.A. Ferguson, S.A. Zygmunt, L.A. Curtiss, Structure-activity relationships for propane oxidative dehydrogenation by anatase-supported vanadium oxide monomers and dimers, J. Catal. 302 (2013) 31–36.
[43] N.E. Damoyi, H.B. Friedrich, H.G. Kruger, D. Willock, Density functional theory studies of the uncatalysed gas-phase oxidative dehydrogenation conversion of *n*-hexane to hexenes, Comput. Theor. Chem. 1114 (2017) 153–164.